A Complete Design of a High Frequency Medium Voltage Multi-Port Transformer

Ahmad El Shafei[1], Saban Ozdemir[1,2], Necmi Altin[1,3], Garry Jean-Pierre[1], and Adel Nasiri[1]
[1]Center for Sustainable Electrical Energy Systems, University of Wisconsin Milwaukee, Milwaukee, USA
[2] Department of Electricity and Energy TBMYO, Gazi University, Ankara, Turkey
[3] Department of Electrical & Electronics Engineering, Faculty of Technology, Gazi University, Ankara, Turkey
aie@uwm.edu; ozdemir@uwm.edu; altin@uwm.edu; jeanpie4@uwm.edu; nasiri@uwm.edu

***Abstract*—In this paper, design of a compact high frequency four-port transformer for a Solid-State Transformer (SST) arrangement is presented. Unlike other SSTs, the four-port system integrates three active sources and a load port with galvanic isolation via a single transformer core. In addition to this feature, one of the three source ports is designed to operate at Medium Voltage (MV) 7.2kV for direct connection to 4.16kV AC grid, while other ports nominal voltages are rated at 400V. The transformer is designed to operate at 50kHz and to supply 25kW/port. Thus, the proposed system connects the MV grid, Energy Storage System (ESS), PV, and DC load to each other on a single common transformer core. Based on the system power demand and availability of renewable energy resources, utility and energy storage ports can either supply or draw power, while PV port can only supply power, maintaining the required demand for the load. This work focuses mainly on the High Frequency Transformer (HFT) design. An extensive study is carried out to obtain the optimal, compact, cost effective, and high efficiency model. Modeling, mathematical, and simulation results are derived and presented to demonstrate the viability of this design.**

Keywords—Multi-port transformer, solid state transformer, medium voltage, microgrid, finite element analysis, co-simulation.

I. INTRODUCTION

At the present time, the utilization of renewable power sources has expanded widely to replace petroleum product-based energy sources [1-3]. Distribution Generation (DG) defined as in the form of solar power, wind power, and biogas power generation, etc. will increasingly penetrate microgrids and future electrical power systems [4]. This penetration has enforced the need for new solutions to integrate AC and/or DC sources and loads. Solid State Transformer (SST) is a promising concept for future microgrid implementation. Basically, the SST is a combination of a medium-or high frequency transformer and a power converter, and it is an alternative to the Line Frequency Transformer (LFT). The AC voltage step up/down functionality is achieved via a medium- or high frequency isolated transformer. Increasing the switching frequency will lead to reduction in transformer bulk size and volume. Moreover, it is a smart plug-and-play interface for exchanging electric power among its ports and can provide superior features [5]. Since it is a fully controlled device, advanced control, protection and monitoring functions can be provided such as voltage and power factor regulation, power flow control, voltage disturbance rejection, load disturbance rejection, etc., which are not available with traditional LFTs [6]. Design of High Frequency Transformers (HFTs) is more complex than the design of LFTs and requires an accurate electromagnetic and loss analysis along with insulation considerations and thermal management.

Recent developments on advanced magnetic materials with low power loss and high saturation flux density as well as high power-high frequency switching devices made it possible to design high efficiency high power density SSTs [7]-[9]. Many studies have been projected lately on SST design [10]-[14]. However, most of these studies are on conventional two-winding transformers. As mentioned earlier, the significant increase in the number of DGs and the importance of smart grid and microgrid concepts has dictated the need for a single compact component integrating multiple sources. This triggered the idea of a Multi-Port Solid State Transformer (MPSST). Few articles and research work have been directed towards this concept [15]-[19]. Since increasing the number of ports increases the control complexity, most of the MPSST studies have focused on three-port systems. In [17], design of a 10kW/port four-port transformer for the SST application is presented. Possible applications of MPSST and volt-VAR control in future distribution systems is proposed [16]. However, all the ports in [16]-[17] are designed to operate at low voltage level.

Generally, Dual Active Bridge (DAB) converters are used at each port of the converter, and the power flow from one port to another is controlled via the phase-shift. However, a change in phase-shift in one converter affects the power flows among all other ports. Therefore, the control of four-port SST is another challenge. To tackle this problem, a Thevenin-equivalent circuit-based control algorithm is proposed to control the power flow and load voltage [20]. The DAB converters used in SST applications use the transformers' leakage inductance as converter inductor. This eliminates the additional inductor requirement and provides a reduction in total size and loss values. Leakage inductance value depends on the core geometry, winding placement, and coupling factors, hence, the transformer model gets more complex and challenging to design. In addition to parameters such as efficiency, energy density, cost, parasitic capacitance, insulation, etc., requirements on the leakage inductance must be also satisfied.

In this study, a complete design of a MV four-port SST rated at 50kHz, 25kW/port is presented. The four ports represent RES

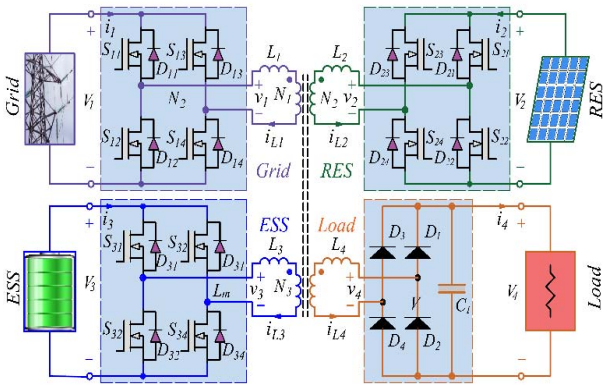

Fig. 1. MV MPSST System.

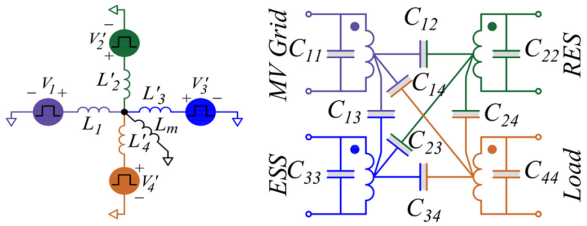

(a) (b)

Fig. 2. a) Equivalent inductance circuit of the transformer referred to port-1, b) Equivalent capacitance circuit.

(e.g. PV), ESS, grid, and load (Fig. 1). Grid port is designed to be at 7.2kV in-order to provide the possibility of integration to 4.16kV AC grid directly, while the other ports are rated at 400V. Three DAB converters are used for PV, ESS and grid ports, whereas a full bridge diode rectifier is used for the load port. Optimal core material selection, windings placement, leakage and magnetizing inductance values, core and winding losses, and parasitic capacitance among the windings are investigated in-order to give the optimal MV MPSST design in-terms of power density, cost and efficiency. In addition, a control method is presented to decouple the power flows among the ports. The transformer design is validated through Finite Element Analysis (FEA) based simulation studies performed with ANSYS-Maxwell-3D and ANSYS-Simplorer, while the proposed control scheme is validated with MATLAB/Simulink simulations.

II. Design and Modeling of The MV MPSST

The complexity that lies behind this concept stems from the fact that there are a lot of parameters and trade-offs to study and carefully choose. For instance, it has multiple windings where each winding has its own leakage inductance and parasitic capacitance as illustrated in Fig. 2(a) and Fig. 2(b), respectively. This paper will discuss the steps that are conducted for the design stage along with FEA simulation for the transients, magnetics, and electrostatics characteristics of the system.

A. Basic Transformer Design

Determining the mechanical dimensions in the HFT is essential since it affects the power density and cost of the transformer. Eq. (1) can be used to calculate the core cross-sectional and window areas:

$$A_P = A_C W_a = \frac{S}{K_f K_{CU} B_m f J} 10^4 \quad (1)$$

here, A_c represents the core cross-sectional area, W_a window area of the core, A_p product of A_c and W_a, S apparent power, K_f waveform coefficient of the excitation voltage, K_{cu} window utilization factor, B_m maximum flux density, f operating frequency, and J current density of the wire. The voltage induced on the transformer windings can be obtained with Faraday's law as given in (2):

$$v(t) = N\frac{d\emptyset(t)}{dt} = NA_C\frac{dB(t)}{dt} \quad (2)$$

here, $v(t)$ is the induced voltage at the transformer winding, $\emptyset(t)$ electromagnetic flux, and N number of turns. As it is well-known, a dead-time is often used for the ON/OFF transitions of the converter switches. By considering this dead-time and rearranging (2) for B_m, (3) can be derived:

$$B_m = \frac{1}{2}\frac{E}{NA_C}\left(\frac{T}{2} - T_d\right) \quad (3)$$

where T denotes the switching period and T_d dead-time. B_m and N are key parameters in transformer design. If B_m is chosen for a specific core by considering core loss and size, then N can be obtained for the given core cross-sectional area, dead-time, waveform factor, operating voltage, and frequency as follows:

$$N = \frac{E}{K_f A_C B_m f}\left(1 - \frac{T_d}{\pi}\right) \quad (4)$$

While lower B_m value decreases core losses, it increases the required core cross-sectional area as well as the total copper amount and winding losses. Therefore, an optimal selection process should be followed. The core losses of a soft magnetic material can be calculated using Steinmetz equation given in (5):

$$P_C = k_{ref} B^{\beta} f^{\alpha} \quad (5)$$

here, P_c is core loss while k_{ref}, α and β are core coefficients which are given in the material product datasheet.

B. Transformer Insulation Design

The insulation standard requirement for a dry-type transformer is described in IEEE Std. C.57.12.01 and IEEE Std. C57.124. The requirement describes how to make Basic Impulse Lightning (BIL) and partial discharge tests. According to these standards, BIL test voltage for this MV MPSST transformer shall be at 30kV. For partial discharge testing, the operating voltage should be increased 1.8-times for a 30-seconds duration, then followed by an increase of 1.3-times for 3-minutes timeframe. At the end of the test, the partial discharge level should be less than 10pC for solid cast winding transformer. In-order to ensure proper insulation between windings, 10kV AC red single polyurethane-nylon (MW80-C) has been used as cables insulation jackets.

C. Core Material and Shape

Selection of the core material based on the design targets (efficiency, power density, and cost) will be a cornerstone for the MV MPSST design. Four material types are commonly used for medium and high frequency transformer applications, namely; Si-Steel, nanocrystalline, amorphous, and ferrite. Table I summarizes the characteristics and tradeoffs for using each of these material types for this application [2], [21], [22,23].

The aim of the design under consideration is the applicability and feasibility of it in the industry. An extensive and thorough

TABLE I: COMPARISON OF CORE MATERIALS

Core Material	Power Loss	Permeability	B_{max}	Cost	Market
Ferrite	Low	High	Moderate	Low	High
Si-Steel	High	High	High	Low	High
Nanocrystalline	Low	High	High	High	Low
Amorphous	High	High	High	Moderate	High

study have been conducted to choose the best material in-terms of tradeoffs and characteristics. It has been concluded that ferrite core is the optimal choice because of its low core power loss, high permeability, low cost, abundance of market availability U/E shapes and sizes, reasonable peak saturation flux density, high coercivity force, and relatively low magnetostriction coefficient. Ferrite 3C94 material from Ferroxcube has been chosen to serve as the core material for the MV MPSST.

Leakage inductance across each port in the DAB topology has major effects on power flow, current shape and value, and therefore, it is used to dictate the power flow between ports. While higher values of leakage inductance limit the power transfer capability, lower values cause high peak current values. This will lead to a reduction in efficiency and makes power converter design more difficult to attain. Thus, keeping the windings leakage inductance at the desired value is a critical requirement in the MPSST design. The Shell-type core is superior to the Core-type one in-terms of confining the flux inside the transformer core and hence decreasing the leakage inductance. Although some E-shape cores are available in the market, their sizes are specific and relatively small. On the other hand, U-shape cores have a larger selection variety in-terms of dimensions and sizes. Hence, and after going over the available 3C94 U-shape cores dimensions, U-93/76/30mm (width/height/depth) was selected to be the best option in-terms of depth and window area.

D. Transformer Parameters Analysis

Based on the MV MPSST design parameters, theoretical analysis has been conducted according to the aforementioned formulations and material specifications. The analysis was carried out on different geometries and winding arrangements. Variations of B_m, core loss (P_c), winding loss (P_w), sum of core and winding losses (transformer losses, P_{tr}), sum of transformer and switching losses (total losses, P_t), and core and copper weight, are plotted and demonstrated with respect to A_c and N as shown in Fig. 3(a)-Fig. 3(f), respectively.

Results show that for the system under study, A_c and N (for low voltage ports) ranging between 34.08-51.12cm^2 and 6-12, respectively, will result in a higher transformer efficiency. However, it was noticed that going above 9 turns will increase the core and copper volumes, and in-return, causes an increase in the cost and a reduction in the power density. These results gave a good building block information and start for the MPSST design. Afterwards, the closest commercially available Ferrite 3C94 core sizes and shapes were used for core shaping in FEA simulations to test and optimize the model. To reduce high skin and proximity effects at high frequencies, Litz wires were used. Moreover, and as mentioned previously, 10kV AC red single polyurethane-nylon (MW80-C) has been used as cables insulation jackets. Therefore, several models have been simulated with different core sizes (34.08-51.12 cm^2), number

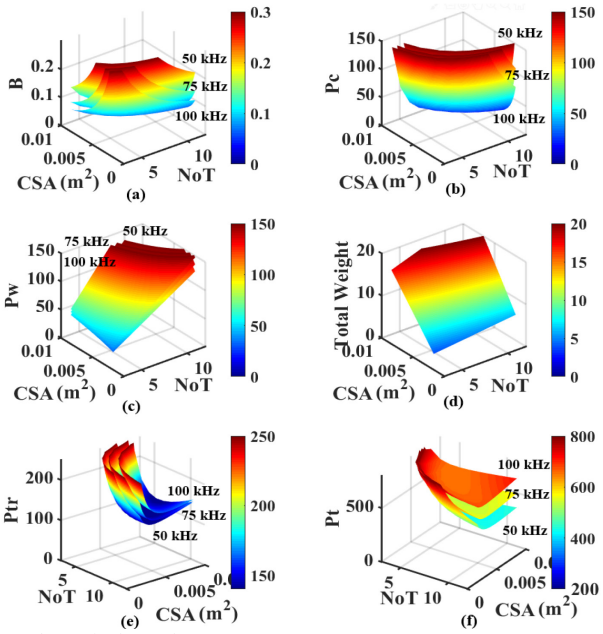

Fig. 3. Theoretical Results: MPSST Parameters vs. N vs. A.

of turns (6-9), and winding arrangements as shown in Fig. 4 and Table II. Each design is modelled in ANSYS-Maxwell-3D, and then co-simulated with a power electronic converter modelled in ANSYS-Simplorer. The transformer is tested for different operating conditions with different phase-shift angles. It should be noted that ANSYS just gives the self and mutual inductance matrix between the four ports and does not calculate the leakage and magnetizing inductance values. Therefore, a systematic and theoretical mathematical derivation has been carried out in-order to calculate these inductances values. The MPSST equivalent circuit was derived and the winding arrangements have been taken into consideration in-order to calculate the leakage inductance for all the models of Fig. 4. This derivation is not the purpose of this paper and thus it will not be presented.

III. CONTROL SYSTEM DESIGN FOR MPSST

Three H-bridge converters and a full-bridge diode rectifier (load port) are used to control the power flow and load voltage of the MPSST. The law that governs the power flow is the same as the DAB converter one. Therefore, power flowing from port-x to port-y can be expressed by (6):

$$P_{xy} = \frac{V_x' V_y'}{2\pi^2 f_s L_{xy}} \phi_{xy}(\pi - \phi_{xy}), \quad \phi_{xy} = \phi_x - \phi_y \qquad (6)$$

here, P_{xy} is the power transferred from port-x to port-y; ϕ_x and ϕ_y are phase shift angles of the converters connected to port-x and port-y, respectively; V_x' and V_y' are DC voltages referred to the AC side of port-x and port-y, respectively; f_s is the switching frequency, and L_{xy} is the equivalent inductance between port-x and port-y.

The system equivalent inductance circuit is shown in Fig. 5. The equivalent inductance values among two ports must be calculated in-order to obtain the delivered power. By neglecting the magnetization inductance, the Thevenin-equivalent inductance between port-1 and port-2 can be written as (7):

$$L_{12} = L_{21} = \frac{L_1 L_3' L_4' + L_1 L_2' L_4' + L_1 L_2' L_3' + L_2' L_3' L_4'}{L_3' L_4'} \qquad (7)$$

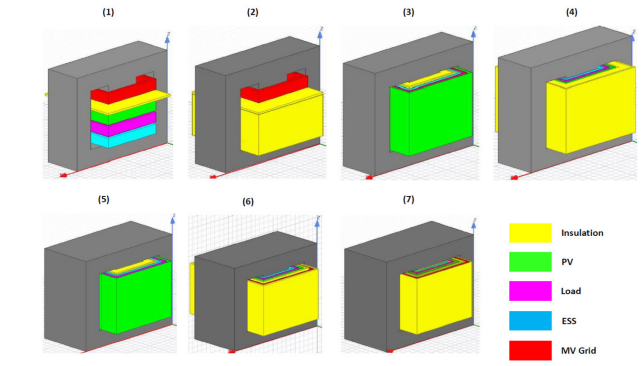

(a)

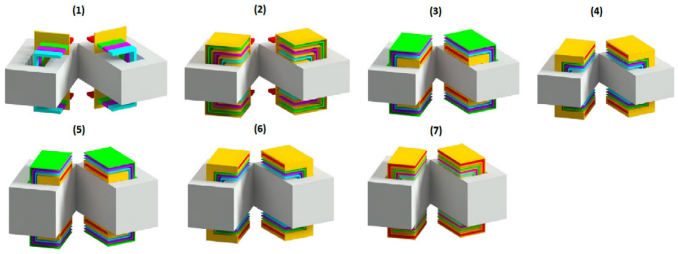

(b)

Fig. 4. Investigated MV MPSST design models: (a) Side View, (b) Cut-out.

TABLE II: MODELS DIMENSIONS

Model No.	1	2	3	4	5	6	7
Shapes Used	8U	8U	8U	8U	12U	12U	12U
Ac (cm^2)	34.1	34.1	34.1	34.1	51.1	51.1	51.1
Volume (cm^3)	1122	1122	1122	1122	1683	1683	1683

here, L_1 is port-1 leakage inductance; and L_2', L_3' and L_4' are leakage inductances of ports-2, 3 and 4 referred to port-1, respectively. Other equivalent inductance values can also be written in the same fashion. Similarly, the Thevenin-equivalent voltages can be written for this circuitry. However, since the Thevenin-equivalent voltage of a port depends on both the sending and receiving ports, it should be calculated for every power flow option. For instance, the Thevenin-equivalent voltage of port-3 is written in (8) and (9) when power flows from port-1 to port-3 and from port-2 to port-3, respectively.

$$v_{TH3_{1-3}} = \frac{L_2'L_4'}{L_2'L_3'+L_2'L_4'+L_3'L_4'}v_3' \quad (8)$$

$$v_{TH3_{2-3}} = \frac{L_1'L_4'}{L_1'L_3'+L_1'L_4'+L_3'L_4'}v_3' \quad (9)$$

According to current directions shown in Fig. 5, the power equations for each port can be written as below:

$$P_2 = P_{12} - P_{23} - P_{24} \quad (10)$$

$$P_3 = P_{13} + P_{23} - P_{34} \quad (11)$$

$$P_4 = P_{14} + P_{24} + P_{34} \quad (12)$$

$$P_1 = -P_2 - P_3 - P_4 \quad (13)$$

Then, by using (6) and (10)-(13), power equations for each port can be obtained. For instance, port-2 power can be written as:

$$P_2 = \frac{V_1V_{TH2_{1-2}}}{2\pi^2 f_s L_{12}}\phi_2(\pi-\phi_2) - \frac{V_2V_{TH3_{2-3}}}{2\pi^2 f_s L_{23}}(\phi_2-\phi_3)(\pi-\phi_2+\phi_3) - \frac{V_2V_{TH4_{2-4}}}{2\pi^2 f_s L_{24}}(\phi_2-\phi_4)(\pi-\phi_2+\phi_4) \quad (14)$$

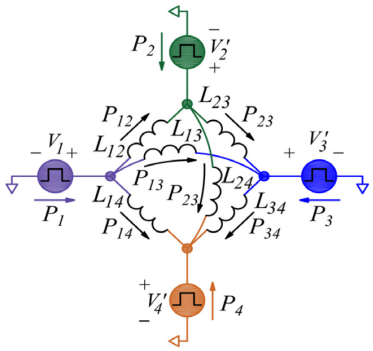

Fig. 5. The equivalent inductance model for the four-port SST.

It is worth noting that the power of each port depends on other ports phase-shift angles. This makes the control of the system very complicated. Hence, a small gain ($x+\Delta x$) linearization method is applied to the power equations to decouple the power equation [24], [25]:

$$P_2 + \Delta P_2 = \frac{V_1V_{TH2_{1-2}}}{2\pi^2 f_s L_{12}}(\phi_2+\Delta\phi_2)(\pi-\phi_2-\Delta\phi_2) - \frac{V_2V_{TH3_{2-3}}}{2\pi^2 f_s L_{23}}(\phi_2+\Delta\phi_2-\phi_3-\Delta\phi_3)(\pi-\phi_2-\Delta\phi_2+\phi_3+\Delta\phi_3) - \frac{V_2V_{TH4_{2-4}}}{2\pi^2 f_s L_{24}}(\phi_2+\Delta\phi_2-\phi_4-\Delta\phi_4)(\pi-\phi_2-\Delta\phi_2+\phi_4+\Delta\phi_4) \quad (15)$$

here, the total power delivered is expressed by two terms; P_x represents the power that depends on V_x, V_y , L_{xy}, V_{xy}, ϕ_x, and ϕ_y, while ΔP_x given in (16) represents the power variation that depends on the phase-shift variation ($\Delta\phi_x$ and $\Delta\phi_y$).

$$\Delta P_2 = \frac{V_1V_{TH2_{1-2}}}{2\pi^2 f_s L_{12}}(-2\phi_2+\pi)\Delta\phi_2 - \frac{V_2V_{TH3_{2-3}}}{2\pi^2 f_s L_{23}}(-2\phi_3+2\phi_2+\pi)\Delta\phi_3 + \frac{V_2V_{TH3_{2-3}}}{2\pi^2 f_s L_{23}}(-2\phi_3+2\phi_2+\pi)\Delta\phi_2 - \frac{V_2V_{TH4_{2-4}}}{2\pi^2 f_s L_{24}}(-2\phi_4+2\phi_2+\pi)\Delta\phi_4 + \frac{V_2V_{TH4_{2-4}}}{2\pi^2 f_s L_{24}}(-2\phi_4+2\phi_2+\pi)\Delta\phi_2 \quad (16)$$

By using $\Delta\phi_x$ and $\Delta\phi_y$ as perturbation control variables, the decoupled power flow control can be achieved in-order to control the power flow. Once ΔP_3 and ΔP_4 are obtained by using the same method above, this can be written in a linear system equation form as below:

$$\begin{bmatrix}\Delta P_2\\ \Delta P_3\\ \Delta P_4\end{bmatrix} = \begin{bmatrix}(a+b+c) & -b & -c\\ -b & (b+d+e) & -e\\ -c & -e & (c+e+f)\end{bmatrix}\begin{bmatrix}\Delta\phi_2\\ \Delta\phi_3\\ \Delta\phi_4\end{bmatrix} = K\cdot\Delta\phi \quad (17)$$

where: $a = \frac{V_1V_{TH2_{1-2}}}{2\pi^2 f_s L_{12}}(-2\phi_2+\pi)$, $b = \frac{V_2V_{TH3_{2-3}}}{2\pi^2 f_s L_{23}}(-2\phi_3+2\phi_2+\pi)$, $c = \frac{V_2V_{TH4_{2-4}}}{2\pi^2 f_s L_{24}}(-2\phi_4+2\phi_2+\pi)$, $d = \frac{V_1V_{TH3_{1-3}}}{2\pi^2 f_s L_{13}}(-2\phi_3+\pi)$, $e = \frac{V_2V_{TH3_{2-3}}}{2\pi^2 f_s L_{23}}(-2\phi_3+2\phi_2+\pi)$, $f = \frac{V_1V_{TH4_{1-4}}}{2\pi^2 f_s L_{14}}(-2\phi_4+\pi)$.

Therefore, the control variable can be calculated depending on the required power variations in accordance to (18).

$$\Delta\phi = K^{-1}\cdot\Delta P \quad (18)$$

I. SIMULATION RESULTS

Simulation of the complete system by linking the Maxwell-3D model (physics and magnetics of the transformer) along with Simplorer circuit (power electronics circuit) will result in a

TABLE III: MODELS PARAMETERS AND SIMULATION RESULTS

Model No.		1	2	3	4	5	6	7
B_{max} (T)		0.26	0.28	0.50	0.26	0.32	0.2	0.17
Parasitic Cap. (pF)	ES	20.7	30.1	109	74.7	126	142	92.3
	Load	30.5	41.4	191	141	219	169	171
	MV Grid	8.3	9.9	44.7	52.5	54.6	61.6	70.4
	PV	19	24.6	130	122	151	91.4	151
Leakage Ind. (µH)	ES	5.9	2.7	905	0.8	905	0.7	1.2
	Load	6.5	2.6	905	0.7	905	0.8	0.8
	MV Grid	7.9	6.6	906	0.8	906	1.0	0.4
	PV	8.3	3.0	162	0.6	162	1.0	0.6
Magnetizing Ind. (µH)		1812	1795	906	1847	906	2735	6065
Losses (W)	Core	16.9	19.1	73.3	17.5	27.4	8.9	15.2
	Winding	74.8	114	172	366	89.1	366	58.2
	Total	91.7	133	246	383	117	375	73.4
Efficiency (%)		99.6	99.5	99	98.5	99.5	98.5	99.7

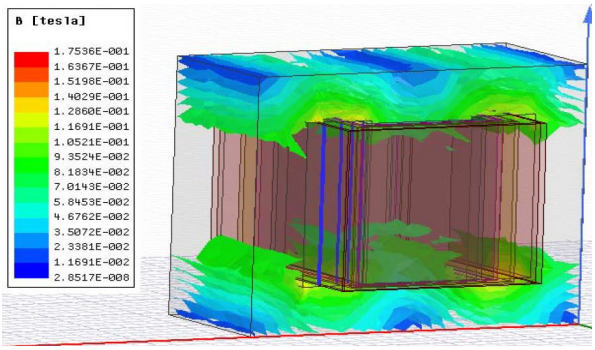

Fig. 6. Core Flux Density Distribution.

complete and realistic simulation of the entire MV MPSST system. After the evaluation of the possible design models for the proposed MV MPPST (Fig. 4), Maxwell-3D/ Simplorer co-simulation studies are carried out. The ports voltages of the system are 7.2kV DC for MV grid port and 400V DC for ESS, PV, and load ports. The simulation is carried out at 50kHz switching frequency and at full load to deliver 25kW to the load port. The duty cycle of the PWM signals are kept constant at 50% and power control is obtained by controlling the phase-shift angles among the H-bridge converters. The obtained results from the simulation studies are presented in Table III. Here, core shape, effective cross-sectional area, volume, transformer losses, and efficiency are given for each model. It is seen that Model 7 provides the lowest leakage inductance with the highest efficiency level. The flux distribution of this model is given in Fig. 6. It is seen that the maximum flux density is around 0.17T which is below the design target limit that is defined by ferrite material specifications. The detailed parameters of the selected optimal model are given in Table IV.

Fig. 7 shows the ports currents and voltages waveforms. As can be seen from the figure, while the PV and grid port currents are in one direction, the load and ESS port currents are in reverse direction. At this instant, the grid and PV ports are delivering power to the load and ESS ports. Many power flow schemes can be analyzed. Based on the systems' power demand, state of ESS, and renewable energy resources availability, the utility and energy storage ports can either supply or draw power, while the PV can only supply power, to maintain the load voltage at its reference value. In-order to test the proposed control scheme, the Simulink model of the suggested control scheme is designed and tested. It is assumed

TABLE IV : OPTIMAL MODEL DETAILED PARAMETERS

Parameter		Value
No. of Turns		9/9/9/162
Litz Wire (AWG)		8/8/8/16
B_{max} (T)		0.175
Parasitic Capacitance (pF)	ES	92.263
	Load	170.918
	MV Utility	70.408
	PV	151.006
Leakage Inductance (µH)	ES	1.254
	Load	0.838
	MV Utility	0.448
	PV	0.604
Magnetizing Inductance (µH)		6064.900
Core Losses (W)		15.222
Winding Losses (W)		58.211
Total Losses (W)		73.430
Efficiency (%)		99.710
Effective Area (cm^2)		51.120
Core Volume (cm^3)		1683

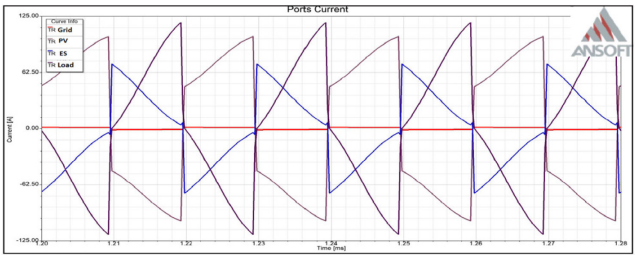

(a)

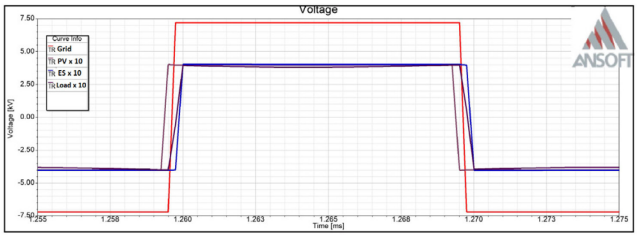

(b)

Fig. 7. MV MPSST Voltages and Currents.

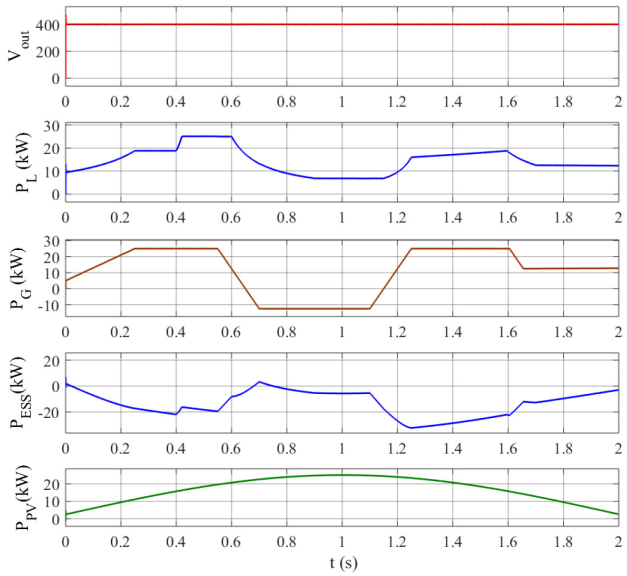

Fig. 8. Output voltage and power waveforms of the proposed MV MPSST.

in the simulations that the Maximum Power Point Tracker (MPPT) is determining the reference power for the PV port. Besides, a random power reference value is applied for the grid port. The proposed controller determines the required phase-shift angles to track the reference powers of the PV and grid ports and to keep the load voltage at its desired value. The simulation results are given in Fig. 8. As it is seen from the figure, the proposed control scheme provides a desirable fast response. It can control the port powers and output voltage and track the reference signals as required.

II. CONCLUSION

In this study, the design of a high frequency MV MPSST system has been presented and simulated. Based on the basic transformer design, 7 design examples are determined. These designs are simulated and evaluated in-terms of efficiency, volume, leakage inductance and parasitic capacitance. The results show that Model 7 provides the optimal performance. Besides, a control scheme which can provide decoupled control of power flows among the ports has been presented and simulated. It is seen that the proposed controller provides fast transient response and control of the port powers and output voltage with high accuracy. The MV MPSST prototype is under construction and the required cooling thermal analysis and implementation will be conducted and built as well.

ACKNOWLEDGMENT

This material is based upon work supported by the National Science Foundation under Grant No. 1650470. Any opinions, findings, and conclusions or recommendations expressed in this material are those of the author(s) and do not necessarily reflect the views of the National Science Foundation. Dr. Necmi Altin and Dr. Saban Ozdemir thank the financial support which they have received from the Scientific and Technological Research Council of Turkey (TUBITAK) BIDEB-2219 Postdoctoral Research program.

REFERENCES

[1] Sefa I., Komurcugil, H., Demirbas, S., Altin N., Ozdemir S., “Three-Phase Three-Level Inverter With Reduced Number of Switches for Stand-Alone Pv Systems”, 6th Int. Con. on Renewable Energy Research and App., ICRERA 2017, 1119-1124, 5-8 Nov. San Diego, CA, USA, (2017).

[2] H. Tumbelaka, E. Muljadi, and W. Gao, “The Impact of Transformer Winding Connections of a Grid-Connected PV on Voltage Quality Improvement”. *International Journal of Renewable Energy Research,* vol. 8, no. 1, March 2018.

[3] Altin, N. Ozdemir, S. and Sefa, I., “A Three-Level MPPT Capability Rectifier For High Power Direct Drive WECS”, The Int. Conf. on Renewable Energy Research and App., ICRERA 2012, Japan, 1–6 (2012).

[4] W. Zhang, S. Zhu, J. Zheng, and H. Zhang. “ Impacts of Distrbuted Generation on Electric Grid and Selecting of Isolation Transformer”. *2005 IEEE/PES Transmission and Distribution Confreference & Exhibition: Asia and Pacific Dalian, China.*

[5] A. Q. Huang and J. Baliga, "FREEDM System: Role of power electronics and power semiconductors in developing an energy internet,"*21st Int. Symp on Power Semiconductor Devices&IC's*, Barcelona, 2009, pp. 9-12.

[6] X. She, X. Yu, F. Wang and A. Q. Huang, "Design and Demonstration of a 3.6-kV–120-V/10-kVA Solid-State Transformer for Smart Grid Application," IEEE Trans. Power Electron. 29 (8), pp. 3982-3996, 2014.

[7] W. Shen, F. Wang, D. Boroyevich and C. W. Tipton, "Loss Characterization and Calculation of Nanocrystalline Cores for High-Frequency Magnetics Applications," *IEEE Transactions on Power Electronics*, vol. 23, no. 1, pp. 475-484, Jan. 2008.

[8] W. A. Reass *et al*., "High-frequency multimegawatt polyphase resonant power conditioning," *IEEE Transactions on Plasma Science*, vol. 33, no. 4, pp. 1210-1219, Aug. 2005.

[9] M. K. Das *et al*., "10 kV, 120 A SiC half H-bridge power MOSFET modules suitable for high frequency, medium voltage applications," *IEEE Energy Conv. Congress and Expo.*, Phoenix, AZ, 2011, pp. 2689-2692.

[10] S. Roy, A. De and S. Bhattacharya, "Current source inverter based cascaded solid state transformer for AC to DC power conversion," *2014 International Power Electronics Conference (IPEC-Hiroshima 2014 - ECCE ASIA)*, Hiroshima, 2014, pp. 651-655.

[11] H. Fan and H. Li, "High-Frequency Transformer Isolated Bidirectional DC–DC Converter Modules With High Efficiency Over Wide Load Range for 20 kVA Solid-State Transformer," *IEEE Transactions on Power Electronics*, vol. 26, no. 12, pp. 3599-3608, Dec. 2011.

[12] T. Zhao, L. Yang, J. Wang and A. Q. Huang, "270 kVA Solid State Transformer Based on 10 kV SiC Power Devices," *2007 IEEE Electric Ship Technologies Symposium*, Arlington, VA, 2007, pp. 145-149.

[13] Hengsi Qin and J. W. Kimball, "Ac-ac dual active bridge converter for solid state transformer," *2009 IEEE Energy Conversion Congress and Exposition*, San Jose, CA, 2009, pp. 3039-3044.

[14] S. Ozdemir, S. Balci, N. Altin and I. Sefa, I., “Design and performance analysis of the three-level isolated DC-DC converter with the nanocyrstalline core transformer”, *International Journal of Hydrogen Energy*, vol.42, no.28, pp.17801-17812, 2017.

[15] A. C. Nair and B. G. Fernandes, "A novel multi-port solid state transformer enabled isolated hybrid microgrid architecture,"*43rd Annual Conf. of the IEEE Ind. Electronics Society*, Beijing, 2017, pp. 651-656.

[16] M. Rashidi, A. Bani-Ahmed,A. Nasiri, "Application of a multi-port solid state transformer for volt-VAR control in distribution systems," *IEEE Power&Energy Society General Meeting*, Chicago, IL, 2017, pp.1-4.

[17] M. Rashidi, A. Bani-Ahmed, R. Nasiri, A. Mazaheri and A. Nasiri, "Design and implementation of a multi winding high frequency transformer for MPSST application," *IEEE 6th Int. Conf. on Renewable Energy Research and Applications*, San Diego, CA, 2017, pp. 491-494.

[18] V. N. S. R. Jakka and A. Shukla, "A triple port active bridge converter based multi-fed power electronic transformer, "*2016 IEEE Energy Conv. Congress and Exposition (ECCE)*, Milwaukee, WI, 2016, pp. 1-8.

[19] W. L. Malan, D. M. Vilathgamuwa, G. R. Walker and M. Hiller, "A three port resonant solid state transformer with minimized circulating reactive currents in the high frequency link,"*2016 IEEE 2nd Annual Southern Power Electronics Conference (SPEC)*, Auckland, 2016, pp. 1-6.

[20] S. Falcones, R. Ayyanar and X. Mao, "A DC-DC multiport-converter-based solid-state transformer integrating distributed generation and storage", *IEEE Trans.Power Electron*., vol.28, no.5, pp. 2192-2203, 2013.

[21] S. Vaisambhayana, C. Dincan, C. Shuyu, A. Tripathi, T. Haonan and B. R. Karthikeya, "State of art survey for design of medium frequency high power transformer," *2016 Asian Conference on Energy, Power and Transportation Electrification (ACEPT)*, Singapore, 2016, pp. 1-9.

[22] S Balci, I Sefa, N Altin, “An investigation of ferrite and nanocrystalline core materials for medium-frequency power transformers”, *Journal of Electronic Materials*, vol.45, no.8, pp. 3811-3821, 2016.

[23] Altin, N., Balci, S. Ozdemir, S. Sefa, I. “A comparison of single and three phase DC/DC converter structures for battery charging”, Renewable Energy Research and Applications (ICRERA), 2013 International Conference on, 1228 – 1233 (2013).

[24] M. Rashidi, N. Altin, S. Ozdemir, A. Bani-Ahmed and A. Nasiri, "Design and Development of a High Frequency Multi-Port Solid State Transformer with Decoupled Control Scheme," IEEE Transactions on Industry Applications. doi: 10.1109/TIA.2019.2939741.

[25] M. Grabarek, M. Parchomiuk and R. Strzelecki, "Conjugated control of triple active bridge converter with common HFT", *11th IEEE Int. Conf. on Compatibility, Power Electron. and Power Eng.*, 4-6 April 2017.